Geophysical Journal International

*Geophys. J. Int.* (2014) **198,** 954–964 doi: 10.1093/gji/ggu173
GJI Geomagnetism, rock magnetism and palaeomagnetism

# Calibration of SQUID vector magnetometers in full tensor gradiometry systems

M. Schiffler,[1] M. Queitsch,[1] R. Stolz,[2] A. Chwala,[2] W. Krech,[2] H.-G. Meyer[2] and N. Kukowski[1]

[1] *Institute of Geosciences Jena, Burgweg* 11, D-07749 *Jena, Germany. E-mail: markus.schiffler@uni-jena.de*
[2] *Leibniz Institute of Photonic Technology Jena, Albert-Einstein-Str.* 9, D-07745 *Jena, Germany*

Accepted 2014 May 12. Received 2014 May 12; in original form 2013 June 28

## SUMMARY

Measurement of magnetic vector or tensor quantities, namely of field or field gradient, delivers more details of the underlying geological setting in geomagnetic prospection than a scalar measurement of a single component or of the scalar total magnetic intensity. Currently, highest measurement resolutions are achievable with superconducting quantum interference device (SQUID)-based systems.

Due to technological limitations, it is necessary to suppress the parasitic magnetic field response from the SQUID gradiometer signals, which are a superposition of one tensor component and all three orthogonal magnetic field components. This in turn requires an accurate estimation of the local magnetic field. Such a measurement can itself be achieved via three additional orthogonal SQUID reference magnetometers. It is the calibration of such a SQUID reference vector magnetometer system that is the subject of this paper.

A number of vector magnetometer calibration methods are described in the literature. We present two methods that we have implemented and compared, for their suitability of rapid data processing and integration into a full tensor magnetic gradiometry, SQUID-based, system.

We conclude that the calibration routines must necessarily model fabrication misalignments, field offset and scale factors, and include comparison with a reference magnetic field. In order to enable fast processing on site, the software must be able to function as a stand-alone toolbox.

**Key words:** Time-series analysis; Numerical solutions; Electromagnetic theory.

## 1 MOTIVATION

Prospection of Earth's magnetic field anomalies is an important tool in, for example, mineral exploration (Macnae 1979), in detection of unexploded ordnance (Barrow & Nelson 1998; Nelson & McDonald 2001; Munschy *et al.* 2007) or in archaeological surveys (Clark 1996; Linzen *et al.* 2009). Such applications often require high spatial and magnetic field resolution for adequate quality of inversion and 3-D modelling. The use of high sensitivity vector magnetometers and/or tensor gradiometers that measure all gradient tensor components is advantageous. Schmidt & Clark 2000 summarize the main advantages of measuring the gradient tensor.

Due to their low intrinsic noise, superconducting quantum interference devices (SQUIDs) are extremely sensitive detectors of magnetic field components (Clarke & Braginski 2004), and of gradient tensor components when appropriately configured. There exist high-sensitivity and high-bandwidth SQUID vector magnetometer instruments (Bick *et al.* 1999; Burghoff *et al.* 2004; Schnabel *et al.* 2004) that allow for prospection of the Earth's magnetic field vector, as well as systems containing both SQUID tensor gradiometers and vector magnetometers. Stolz *et al.* (2006) introduced a Full Tensor Magnetic Gradiometry (FTMG) system for recording all components of the magnetic field and the independent tensor gradient components, with high resolution. This instrument, named JeSSY STAR, was developed at the Institute of Photonic Technology (IPHT) in Jena. The system contains planar-type first-order gradiometers that provide a high intrinsic balance or suppression ratio of the homogeneous magnetic field. Due to fabrication limitations of these gradiometers, measurement of any magnetic gradient component $B_{ik} = \partial B_i / \partial x_k$ becomes superposed with small proportions of the three magnetic field components $B_j$ weighted by certain orthogonal areas called parasitic areas $A_{\mathrm{par},ikj}$:

$$B_{ik}^{\mathrm{meas}} = B_{ik} + \sum\nolimits_j \alpha_{ikj} B_j \text{ with } i, j, k \in (x, y, z) \tag{1}$$

The factors $\alpha_{ikj} = A_{\mathrm{par},ikj} / (b \cdot A)_{ik}$ represent the inverse intrinsic balance of the gradiometer, a measure of suppression of the corresponding homogeneous magnetic field component. With an ideal gradiometer, the balance would reach infinity. The parameters $b$ and $A$ are the baseline and the sensing area respectively of one of the individual pickup loops of the gradiometer (Stolz 2006). Therefore, a SQUID based FTMG system requires a vector magnetometer measuring in the same reference frame as the gradiometers. According to eq. (1) the intrinsic balance of the individual gradiometer can be further enhanced via appropriate data post-processing.

In general, SQUID vector magnetometers require a precise calibration that produces a sensor-to-sensor alignment and simultaneously estimates a set of scale factors reflecting the specific sensitivity of each sensor to its magnetic field component. Additionally, because SQUIDs provide only a relative measure of the magnetic field component, the calibration has to determine the offset value of each sensor. For this purpose often a series of measurements in different spatial orientations is used. Calibration of vector magnetometers is a well-known problem in ship navigation, and many calibration techniques have been presented in the literature (e.g. Merayo *et al.* 2000; Olsen *et al.* 2001; Alonso & Shuster 2002, and others). Here, the methods presented in Olsen *et al.* (2001) and Merayo *et al.* (2000) are applied to the recorded signals of SQUID vector magnetometers and compared in order to assess their suitability for handling misalignments, scaling errors and offsets. These methods were initially developed for satellite-based magnetic mapping missions (Marklund *et al.* 2001; Sabaka *et al.* 2004); and therefore it is assumed that these mature routines reflect an error model appropriate to SQUID magnetometers such that a robust calibration is obtained.

The calibration routines are intended to become part of a daily fieldwork processing toolbox. The numerical details of this work show how the methods can be implemented such that they run efficiently and robustly in the sense that the correct calibration coefficients can be estimated with least restrictions as possible. To check that, the evaluation is performed on a FTMG survey data set acquired with the JeSSY STAR system. The instrument used in this survey will first be described briefly. In the subsequent section the chosen calibration methods approaches are recapitulated and adapted to the calibration of SQUID vector magnetometer data. Finally, the numerical precautions for the particular implementation of these routines are described.

The chosen magnetometer calibration methods require a magnetic reference field. Here we implemented a toolbox which calculates the reference for each particular survey from harmonics coefficients used in the International Geomagnetic Reference Field (IGRF, Finlay *et al.* 2010) or in the High Definition Geomagnetic Model (HDGM, Maus & Manoj 2010). The description of the reference field calculation is followed by application of the adapted calibration methods to an example case data set. Finally, performance of the methods, as well as implementation and the choice of reference field are discussed with respect to the presented case.

## 2 SETUP OF THE MEASUREMENT SYSTEM UNDER OPERATION

Here, we give a brief overview of the system actually used, which is the JeSSY STAR system already introduced (Stolz *et al.* 2006). All SQUID sensors were produced in the Nb/$AlO_X$/Nb thin-film technology at IPHT in Jena (Stolz *et al.* 1999). The JeSSY STAR system consists of a set of six first-order SQUID gradiometers and a triple of lower sensitivity reference SQUID magnetometers used for the reduction of the parasitic response to the magnetic field itself in a post-processing procedure which is called balancing (Vrba 1996). The gradiometer arrangement enables the reduction of the system noise on the measurements and ensures that all linearly independent tensor components can be calculated. The system actually returns six gradient signals, but any set of five can be used to derive a full tensor of the magnetic field gradient.

The three magnetometers are orthogonally mounted onto a small cube (1 $cm^3$) in order to measure the magnetic field vector.

The entire setup is mounted inside a cryostat (a cooling unit) and immersed into liquid helium at 4.2 K. The sensor signals are recorded using 24-bit analogue-to-digital-converters. As intended for a range of $\pm 100$ μT, this system yields an accuracy of $\approx 12$ pT. The data acquisition system contains a high-precision inertial measurement unit (IMU) consisting of three orthogonally oriented gyroscopes and three accelerometers as well as a differential GPS receiver. These units provide information about attitude given by the *Euler* angles (Shin 2005; Shin & El-Sheimy 2007) and position of the measurement system during airborne operation. The *Euler* angles are used to transform the recorded data into a local or Earth-centred-Earth-fixed (ECEF) coordinate system.

## 3 CALIBRATION METHODS FOR VECTOR MAGNETOMETERS

Vector magnetometer calibration obtains a system of equations for transformation of the three magnetometer readings into three magnetic field vector components in the corresponding measurement coordinate system, which is tracked together with the system during motion. It should take into account the non-orthogonality of the three axes described by the orientation of magnetometer antennae, the scaling factor from the magnitude of the magnetic field vector component to the corresponding sensor signal, and the offsets of the magnetometers. SQUIDs can provide only relative magnetic field values since their operation requires a feedback loop (Clarke & Braginski 2004), and the offset is set at the start of the feedback operation.

There are different calibration methods, for example, described in Bonnet *et al.* (2009), Olsen *et al.* (2001), Alonso & Shuster (2002) and Merayo *et al.* (2000). Two of them attracted our particular interest for magnetometer calibration.

### 3.1 Method (a): Vector magnetometer calibration after Olsen *et al.* (2001)

This method was originally developed for the Ørsted satellite mission magnetometers (Olsen *et al.* 2001) and adapted later by Munschy *et al.* (2007). Here, we briefly introduce our adaptation of it.

Olsen *et al.* (2001) initially introduced a set of nine parameters as in eq. (5) describing the raw measurement data $\vec{F} = (F_x, F_y, F_z)^T$ by $\vec{F} = \hat{S} \cdot \hat{D}_{\text{dist}} \cdot \vec{B} + \vec{O}$ as a function of the magnetic field $\vec{B} = (B_x, B_y, B_z)^T$ where $\hat{S} = \text{diag}(s_x, s_y, s_z)$ is the sensitivity matrix consisting of the three scale factors, the quantity $\hat{D}_{\text{dist}}$ is the distortion matrix (4), and $\vec{O} = (o_x, o_y, o_z)^T$ is the vector of the three sensor offsets. The calibration is then done by minimizing the value

$$\chi^2 = \sum (B - B_{\text{ref}})^2, \tag{2}$$

where

$$B = \sqrt{\left(\vec{F} - \vec{O}\right)^T \left(\hat{D}_{\text{dist}}^{-1} \hat{S}^{-1}\right)^T \left(\hat{D}_{\text{dist}}^{-1} \hat{S}^{-1}\right) \left(\vec{F} - \vec{O}\right)} \tag{3}$$

is the total magnetic intensity (TMI) of the measured magnetic field and $B_{\text{ref}}$ is the reference field magnitude (IGRF or HDGM).

In our case, the offsets of the three magnetometers are arbitrary due to the readout circuitry of DC SQUIDs. Their sensitivities account for the transformation of magnetic field readings into a voltage recorded by the data acquisition system. The misalignment error produced from non-orthogonal sensitive axes (caused by the mounting accuracy of the magnetometer triplet on the cube) is described by the distortion matrix $\hat{D}_{\text{dist}}$ (eq. 4). This matrix is a transformation between an ideal orthogonal coordinate system and the non-orthogonal sensor system:

$$\hat{D}_{\text{dist}} = \begin{pmatrix} \sqrt{1 - \sin^2 \alpha_{xy} - \sin^2 \alpha_{xz}} & \sin \alpha_{xy} & \sin \alpha_{xz} \\ \sin \alpha_{xy} & \sqrt{1 - \sin^2 \alpha_{xy} - \sin^2 \alpha_{yz}} & \sin \alpha_{yz} \\ \sin \alpha_{xz} & \sin \alpha_{yz} & \sqrt{1 - \sin^2 \alpha_{xz} - \sin^2 \alpha_{yz}} \end{pmatrix}, \tag{4}$$

where $\alpha_{xy}$, $\alpha_{xz}$ and $\alpha_{yz}$ are the three misalignment angles. Comparing to the original form described in Olsen *et al.* (2001) this should lead to transformation of the magnetometer readings into the correct magnetic field vector components with respect to the measurement coordinate frame. Up to now there is no scalar magnetometer implemented in the JeSSY STAR instrument. Therefore, the reference field is calculated from the IGRF or HDGM for the geographic coordinates of the survey site and the calibration is done by minimizing eq. (2) which depends on the parameter set

$$\vec{p} = (\alpha_{xy}, \alpha_{xz}, \alpha_{yz}, s_x, s_y, s_z, o_x, o_y, o_z). \tag{5}$$

### 3.2 Method (b): Vector magnetometer calibration after Merayo *et al.* (2000) and Bonnet *et al.* (2009)

Instead of comparing the TMI calculated from the magnetometer signals with the one from a reference field, the Merayo method (Merayo *et al.* 2000) uses the fact that the three orthogonal components of $\vec{B}$ measured by ideal magnetometers should appear on the surface of a sphere with radius $B = \left|\vec{B}\right|$ in a Cartesian coordinate system. Here, errors in scale factors $\hat{S}$ transform the sphere into an ellipsoid. The misalignment and offset errors lead to a rotation and a translation of the centre point of the ellipsoid in space, respectively. The task to be solved by calibration is to find the ellipsoid parameters given by

$$(\vec{M} - \vec{c})^T (\hat{U}^T \hat{U})(\vec{M} - \vec{c}) = 1, \tag{6}$$

where $\vec{M}$ is the vector of the magnetometer readings, $\hat{U}$ (eq. 9) an upper triangular matrix, and $\vec{c}$ is the ellipsoid centre. After obtaining the matrices $\hat{U}$ and $\vec{c}$, the calibrated and normalized measurement values are

$$\vec{B} = \hat{U}(\vec{M} - \vec{c}). \tag{7}$$

For fast determination of $\hat{U}$ and $\vec{c}$ eq. (6) is rewritten to a linear parameter form

$$\begin{pmatrix} M_x^2 & M_y^2 & M_z^2 & M_x M_y & M_x M_z & M_y M_z & M_x & M_y & M_z \end{pmatrix} \vec{p} = 1 \tag{8}$$

with the parameter set $\vec{p} = (p_1 \dots p_9)$ (Bonnet *et al.* 2009) reflecting the unknowns in $\hat{U}$ and $\vec{c}$. According to Merayo *et al.* (2000), Barraud & Lesecq (2008) and Bonnet *et al.* (2009) $\hat{U}$ is returned by Cholesky factorization of the matrix

$$\hat{A} = \hat{U}^T \hat{U} = \begin{pmatrix} p_1 & p_4/2 & p_5/2 \\ p_4/2 & p_2 & p_6/2 \\ p_5/2 & p_6/2 & p_3 \end{pmatrix} \tag{9}$$

and the ellipsoid centre can be calculated by $\vec{c} = -\frac{1}{2} \hat{A}^{-1} (p_7, p_8, p_9)^T$. The equation $\hat{D}' \vec{p}' = 0$ is solved by a singular value decomposition (SVD) in order to determine $\vec{p}' = (p_1 \dots p_9, p_{10})$, where $p_{10} = \vec{c}^T \hat{A}^{-1} \vec{c} - 1$. The processing scheme is described in detail for instance in Bonnet *et al.* (2009).

In contrast to Merayo *et al.* (2000), we neglect all soft and hard iron effects since such materials are not located close to the magnetic sensors in our measurement system.

## 4 IMPLEMENTATION OF THE CALIBRATION ROUTINES

As pointed out earlier, the Olsen calibration method with our modifications on SQUID vector magnetometer signals requires an implementation of a reference magnetic field. This procedure is contained in standalone rapid data processing and quality control software for FTMG surveys. The general outline of the algorithms relies on the calculation of the harmonic potential series (Jacobs 1987)

$$V_i = a \sum_{n=1}^{N} \sum_{m=0}^{n} \left(\frac{a}{r}\right)^{n+1} \left(g_n^m \cos m\varphi + h_n^m \sin m\varphi\right) P_n^m(\cos\theta) \tag{10}$$

for a set of geographic coordinates (latitude $\theta$, longitude $\varphi$ and altitude $h$), where $a$ is Earth's mean radius, $r = a + h$, $g_n^m$ and $h_n^m$ are the Gauss–Schmidt coefficients available (NGDC 2012a,b) for the IGRF ($N = 13$) or the HDGM ($N = 729$). The derivation of the magnetic field vector components from eq. (10) delivers the respective reference field for the vector magnetometer calibration task.

In order to perform the calibration we followed two different approaches. In the first approach, the measured magnetic field components of the time series acquired by the moving sensor system were compared with the calculated reference field components. This was done by rotating the reference field components into the measurement coordinate system using the geographic coordinates and *Euler* angles (Fig. 1) derived from the IMU.

The comparison shows smaller differences caused by diurnal variations of the Earth's magnetic field and larger differences caused by insufficient accuracy of the *Euler* angles derived from the IMU signals. Although the performance of our IMU is generally good enough for navigation purpose, the *Euler* angles therein derived typically have inaccuracies of the order of 0.1°. Hence, motion noise on the order of one hundred nanoteslas is superimposed on the magnetic field components. This noise contribution is clearly visible in the magnetic field components rotated into the ECEF in Fig. 2, and is due primarily to the influence of roll and pitch angle changes. Therefore, we conclude that rotation of magnetic field vector components into the ECEF using IMU data yields precision levels four or five orders of magnitude worse than the intrinsic SQUID precision levels.

This observation forces us to the second approach. Returning to the original calibration idea described by Olsen *et al.* (2001), the TMI—as rotational invariant of the magnetic field—is calculated on the one hand from the reference field ($B_{\text{ref}}$) and on the other hand from the magnetometer readings ($B$). Eq. (2) is used to minimize the difference between them in dependence of the parameter set $\vec{p}$.

For successful numerical implementation of this method, the following important aspects have to be taken into account:

(i) The minimization of eq. (2) in dependence on the parameter set $\vec{p}$ is performed via a quasi-Newton algorithm using a cubic line search procedure. The algorithm implements the Limited-memory Broyden–Fletcher–Goldfarb–Shanno (L-BFGS) (Broyden 1970) method for updating the Hessian matrix.
The whole calibration is implemented in MATLAB® with the fminunc function call or external package minFunc (Schmidt 2012).

(ii) On the one hand, the magnitudes of the misalignment angles and scale factors have magnitudes below 5 and the offsets on the other hand are measured in nT ($\approx 10^4$). The minimization routine uses finite difference gradient calculation for pointing towards the minimum. Therefore, a modification of each parameter value $p_i$ of a fixed $\varepsilon$ during the minimization process leads to a significantly smaller change in offsets than in the distortion or sensitivity. For a good minimization ensuring the correct offset values and an equal gradient calculation of all elements of $\vec{p}$, the offset values are internally downscaled to the unit of ten or hundred nT.

(iii) In order to fit the measured to the calculated reference TMI we use the standard deviation as minimization criterion as a modification to eq. (2):

$$\sigma = \sqrt{\frac{\chi^2}{n-1}} = \sqrt{\frac{\sum (B - B_{\text{ref}})^2}{n-1}}, \tag{11}$$

where $n$ is the number of measured samples. After a successful minimization process this standard deviation should reflect magnitude of the actual anomalies with respect to the background reference field. If the calibration process returns $\sigma$ considerably lower or higher than the expected value of the anomaly, for example, too close to zero, the rescaling should be revisited and the routine be run again. A careful quality check or further a priori knowledge about the setting will enhance the results.

In contrast to Olsen's routine, the first approach in comparing the individual measured and reference magnetic field *components* is essential for successful calibration using the method (b) after Merayo *et al.* (2000) and Bonnet *et al.* (2009). In this algorithm only a fit of the ellipsoid eq. (6) via SVD to the measurement data and subsequent application of eq. (7) is performed and therefore neither the correct scale factors $s_i$ nor the correct offsets $o_i$ can be obtained. Therefore, an initial least square fit to the model $\vec{F} = \hat{S} \cdot \vec{B} + \vec{O}$ is performed. The misalignment errors are neglected in this first raw calibration. The reference field vector is rotated into the measurement system's coordinate frame via application of $\vec{B}_{\text{ref},b} = \hat{D}^b_{\text{NED}} \cdot \vec{B}_{\text{ref}}$ where $\hat{D}^b_{\text{NED}}$ is the appropriate rotation matrix (Goldstein 1980) containing the *Euler* angles. Then a linear regression is performed to fit the therein measured magnetometer readings to the vector $\vec{B}_{\text{ref},b}$. Subsequently, the SVD-based

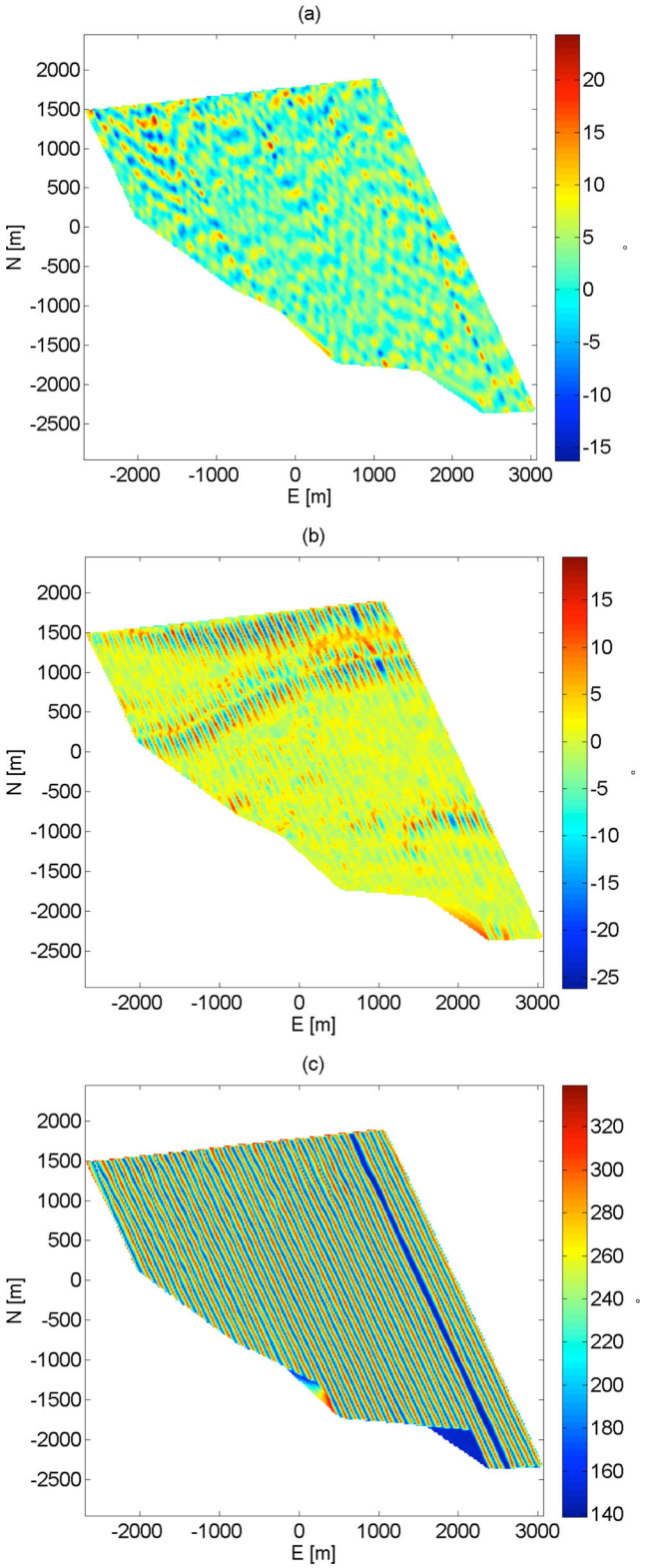


**Figure 1.** Euler angles of the measurement system's attitude during the survey: (a) roll, (b) pitch and (c) heading angle.

calculation of $\hat{U}$ and $\vec{c}$ estimates the misalignment and the correction of the residual scale factor and offset errors. Finally, the calculation of the resulting sphere provides only normalized magnetic field vector components and thus makes it necessary to multiply the results with the reference field magnitude which is obtained from the total intensity corresponding to the IGRF or HDGM model for the present geographic coordinates.

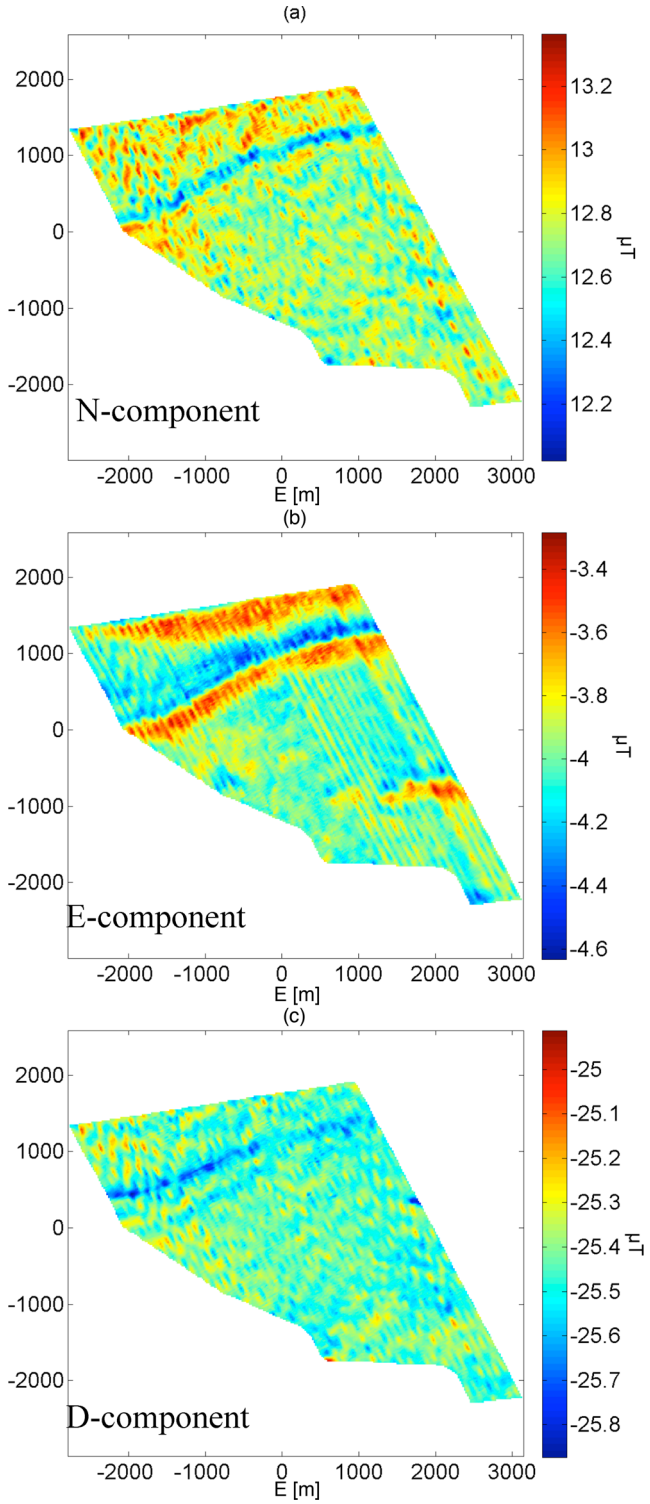


**Figure 2.** (a) Northward ($x$) component, (b) Eastward ($y$) component, (c) Downward ($z$) component of the magnetic field vector of a survey in South Africa (RSA) obtained after calibration by Olsen method. The scanned area is discussed in the subsequent results.

## 5 CASE STUDY FOR EVALUATION OF CALIBRATION METHODS

The newly implemented vector magnetometer calibration methods introduced above are assessed in detail on data obtained in an airborne magnetic survey with the FTMG system mounted in a nonmagnetic towed body underneath a helicopter (Stolz *et al.* 2006). The study area is located in the Republic of South Africa in the Northern Province between Groblersdal and Loskop Dam on the Southeast flank of the Dennilton Dome and represents an area of about 5 km × 5 km. The towed system had in minimum 30 m ground clearance and a line separation

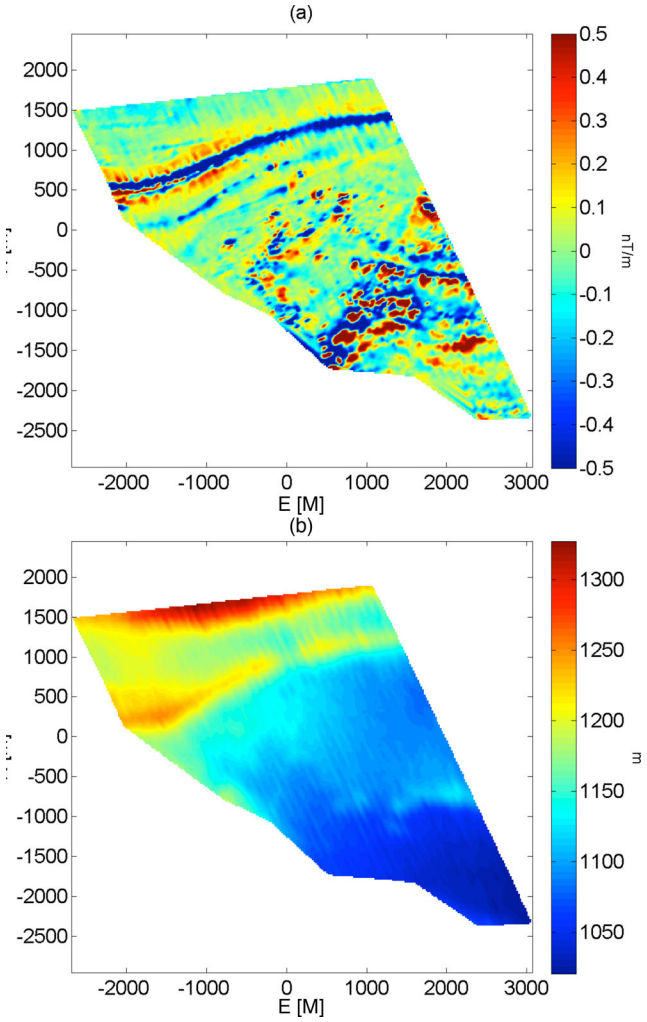


**Figure 3.** Vertical gradient of the vertical magnetic field component (a) and measurement altitude (b) for the survey in RSA.

of 50 m was chosen. The survey was accomplished in two flights on one day. According to the magnetic gradients and altimeter readings (Fig. 3) obtained during this survey, the acquired data set offers low magnetic noise amplitudes, smooth topography, and only a few distinct anomalies. Thus, the test conditions appeared to be well-suited for this experiment.

The residual occurrence of motion noise in the calculated TMI from the measured SQUID vector magnetometer data, represented by its correlation to the calculated *Euler* angles, is a measure for the success of the magnetometer calibration. Any measurement error would lead to response to motion noise in the TMI. As the calibration routines are benchmarked for application to any SQUID magnetometer survey, the test was performed on low-noise data with usual ground clearance but few anomalies, thus enabling a meaningful check for recurring noise.

Here, we focus just on the general methodological description of the new processing algorithms. The presented data serve as a suitable field example demonstrating typical ranges of variation of the error parameters and computational time for the particular implementation. For a general overview of the geological setting at the test site which is formed by the Transvaal Sequence and Bushveld Complex, refer to Crous (1997).

The first calibration approach using Olsen's method leads to the TMI presented in Fig. 4.

Each of the three scale factors $s_i$ and offsets $o_i$ are pre-initialized using a least-square fit of the measurement data to the IGRF rotated into the body coordinate system. The rotation matrices (Goldstein 1980) for this conversion contain *Euler* angles calculated via Kálmán filtering techniques (Shin 2005; Shin & El-Sheimy 2007) from measured IMU data. The three misalignment angles are initially set to zero. The resulting parameter sets of the calibration algorithm for the two survey flights in the study area are shown in Table 1. The residual correlation coefficients of the TMI to the *Euler* angles are −0.07 per cent for the roll angle, 1.48 per cent for the pitch angle and 4.72 per cent for the heading angle, the standard deviation for the individual flights was decreased from 21.5 μT to 51 nT and from 21.9 μT to 41 nT, respectively. These are the numbers of the standard deviation of the anomalies which would be obtained by additional TMI measurements for this area.

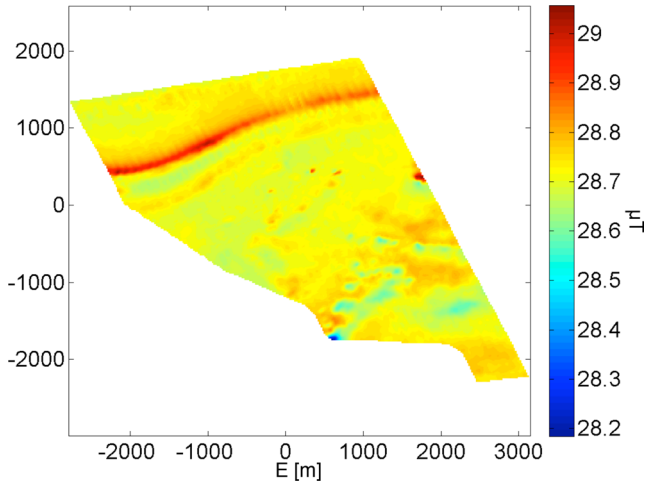


**Figure 4.** TMI obtained by a calibration after Olsen of the survey in RSA. The standard deviation in the study area is $\sigma = 43$ nT.

**Table 1.** Minimization parameters for the sample survey for the Olsen calibration method.

| Flight no. | $\alpha_{xy}$ (°) | $\alpha_{xz}$ (°) | $\alpha_{yz}$ (°) | $s_x$ | $s_y$ | $s_z$ | $o_x$ (μT) | $o_y$ (μT) | $o_z$ (μT) |
|---|---|---|---|---|---|---|---|---|---|
| 1 | 0.37 | −2.36 | −0.42 | −0.501 | 0.511 | −0.518 | 4.67 | −2.06 | −14.24 |
| 2 | 0.42 | −2.27 | −0.56 | −0.501 | 0.504 | −0.516 | 6.38 | −1.38 | −13.70 |

For the calibration with the Merayo method it is necessary to know the alignment of the magnetometer cube with respect to the IMU. After a first rescaling of the magnetometers and subtracting a raw least-squares approximation of the offset, the determination of $\hat{U}$ and $\vec{c}$ is carried out. The results for the two individual flights are:

$$\hat{U}_1 = \begin{pmatrix} 0.3337 & -0.0048 & 0.0334 \\ 0 & 0.3163 & -0.0188 \\ 0 & 0 & 0.2979 \end{pmatrix} \times 10^{-4}\ \mathrm{nT}^{-1}$$

and

$$\hat{U}_2 = \begin{pmatrix} 0.3334 & -0.0067 & 0.0305 \\ 0 & 0.3209 & -0.0148 \\ 0 & 0 & 0.2974 \end{pmatrix} \times 10^{-4}\ \mathrm{nT}^{-1},$$

as well as $\vec{c}_1 = (-2.73, 1.86, 4.72)^T$ μT and $\vec{c}_2 = (-2.60, 1.46, 4.76)^T$ μT. After application of eq. (6) to the measured data, we observe a TMI shown in Fig. 5. Table 2 shows the pre-calibration values of offset and scale. For this pre-calibration a linear least-squares approach was used without determination of the alignment to the IMU.

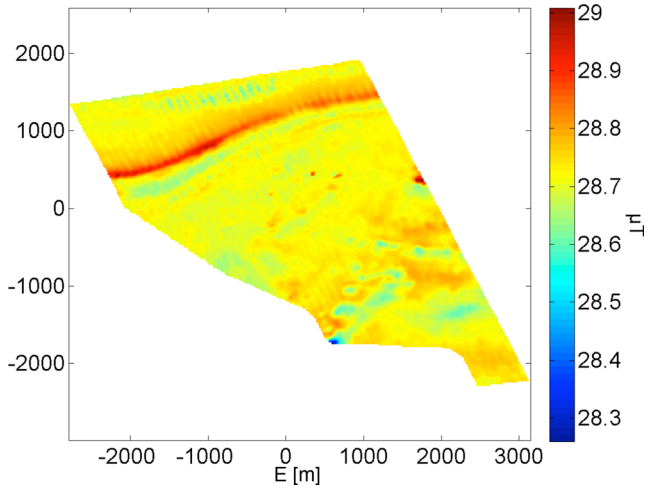


**Figure 5.** TMI obtained after Merayo calibration. The standard deviation in the study area is $\sigma = 47$ nT.

**Table 2.** Sensitivities and offsets for pre-calibration using least-square fit for Merayo calibration method.

| Flight no. | $s_x$ | $s_y$ | $s_z$ | $o_x$ (μT) | $o_y$ (μT) | $o_z$ (μT) |
|---|---|---|---|---|---|---|
| 1 | −0.511 | 0.491 | −0.514 | 3.69 | −1.92 | −14.17 |
| 2 | −0.509 | 0.493 | −0.512 | 5.37 | −1.20 | −13.63 |

## 6 COMPARISON AND ASSESSMENT OF THE CALIBRATION RESULTS

The deviations in the minimization parameters due to effects caused by the particular magnetometer system have been evaluated; then the selected reference field information is estimated; and finally, both calibration methods are compared with respect to usability and computational time.

### 6.1 Olsen method

The scale factors $s_i$ differ only in a range of 0.01 (Table 1) and the misalignment angles $\alpha_{ij}$ differ only in a range 0.1° between both flights for the Olsen magnetometer calibration methods. Ideally, these values should be constant; at least the change of the misalignment angles should be lower than 0.01° for a specific measurement system. It should be noted that a full thermocycle to room temperature and back to operation temperature of 4.2 K will cause changes in scaling and misalignment angles for the SQUID sensors due to mechanical stress. During data acquisition performed for this study the sensor setup was kept cool throughout the survey. Therefore, it is possible that temperature variations and relative motions in the towed bird's interior system components could cause the observed effect. As the first survey flight was undertaken early in the morning while the second was flown at noon, on the one hand the temperature changes could reflect the respective conditions. Further investigations are necessary to clearly identify the source of the deviations.

On the other hand, these parameters are obtained using a gradient-supported minimization process. Therefore the differences in these values also reflect the numerical accuracy of the result of finding the optimized standard deviation. Reflecting the different anomaly roughness in the right- and left-hand half of Fig. 3, the standard deviations of the residual TMI differ for both flights. Because the minimization affects to such changes, it is a better approximation to take the averages of the values for $s_i$ and $\alpha_{ij}$ which is discussed below. From the here presented state it remains not discriminated whether these small derivations primarily originate from the instrument drifts or the minimization inaccuracies of Olsen's method.

The differences in the offsets $o_i$ are due to the readout of the SQUID sensors leading to arbitrary DC values for the signal output. At begin of the data acquisition the feedback loop of each SQUID is closed. At this moment in time the output of all SQUIDs is zero independently of the magnetic field amplitude. Hence the SQUIDs measure an accurate relative value of the corresponding magnetic field component.

### 6.2 Merayo method

Using the Merayo method, the same behaviour is observed in the upper triangular matrix. Here changes are very small. The differences in the ellipsoid centre position are in maximum 400 nT. Nevertheless, this is accomplished as a result of a pre-calibration which shows essentially the same behaviour in the offsets.

A stationary magnetic base station was not installed for this survey. For SQUID FTMG surveys the vector magnetometer readings are principally used for balancing the gradiometer signals; while the main information is derived from the tensor components of the magnetic field gradient. For such surveys, no magnetic base station is necessary since gradiometers with sufficient suppression of the homogeneous Earth magnetic field are not sensitive to diurnal effects: they already measure a difference signal from two magnetometer areas. Furthermore, in airborne measurement as the data set presented here, each flight data set is divided into individual flight lines, each acquired within less than three minutes. Therefore any temporal magnetic variations that occur during a given flight would be averaged into the individual offset—calculated with one of the presented methods—for that line. In fact, offsets of SQUID magnetometers often change arbitrarily even within an operation turn, thus making line-by-line offset determination necessary.

### 6.3 Reference field

As the reference field used in this compilation (Maus & Manoj 2012) is described by globally valid spherical harmonic coefficients it can be easily calculated for each measurement sample point, for the survey midpoint, or for an evenly spaced grid covering the survey area. In Maus & Manoj (2012), the spatial resolution of the IGRF is cited by approximately 1500 km and of the HDGM approximately 28 km. These values are larger than typical SQUID magnetometer surveys used for high-resolution mapping of specific interesting areas. Therefore, a sampling of one point per square kilometre and subsequent interpolation to each survey sample point returns an adequate reference field. Midpoint values for the discussed case study are shown in Table 3. The regression was performed to the respective IGRF values for the first test discussed herein. With respect to motion noise patterns, using HDGM instead of IGRF does not show significant differences in the calibration results although average curvature (see Table 3) is slightly different and the amplitude of both reference fields calculated for the midpoint deviates

**Table 3.** Comparison between IGRF and HDGM reference field values. These components are calculated for the mean geographic coordinates.

| Model | $B_x$ (nT) | $B_y$ (nT) | $B_z$ (nT) | Curvature |
|---|---|---|---|---|
| IGRF | 12 578.69 | −3987.71 | −25 505.30 | 1.8 km$^{-1}$ |
| HDGM | 12 639.59 | −3999.88 | −25 396.09 | 2.0 km$^{-1}$ |

at about 100 nT for the downward component. The standard deviation of the curvature (Gray 1997) for our calibrated data in this example is 52.6 km$^{-1}$.

### 6.4 Comparison of methods

One advantage of the Olsen method is that the rotation of the components of $\vec{B}$ and $\vec{B}_{\text{ref}}$ into a common coordinate system is not necessary because only the TMIs of measured and reference magnetic field components are compared. On the other hand, this prevents us from obtaining detailed information on the alignment of the SQUID magnetometer triplet relative to the coordinate frame of the inertial measurement unit. However, this can be performed after the calibration in a separate minimization routine, for example, to decrease the correlation of the motion noise signal to magnetic field components or by comparison between the measured values to those obtained from TMI for instance by Hilbert transforms. The mathematical methods for these transforms will be presented in a subsequent paper.

The disadvantage of the Olsen method is the dependence of the convergence of minimization on the choice of the aforementioned offset scaling factor. On the one hand, the calibration is a process of parameter estimation based on the minimization of a standard deviation, which is driven towards zero as the parameters converge on an estimate. On the other hand, the standard deviation reflects the difference between the measured and the reference field TMI. Due to the smooth character of the reference, which can be approximated as a spatially constant value, this standard deviation effectively becomes a measure of the anomaly strength for the survey area which has a finite and nonzero value. The LBFGS minimizer therefore requires termination tolerances for the parameter changes and the gradient values. Else the minimization diverges and non-realistic values (e.g. for the misalignment angles) are determined. Additional information from previously performed TMI surveys on the one hand could improve the regression and the quality of the TMI obtained after calibration of our measurement data. But, different processing (e.g. filters and specific subtraction of reference field values therein) could on the other hand lead to misleading results. As the presented routines are intended to be self-contained and, except of the reference field coefficients, to be used standalone without further information, the acquired quality meets the above discussed goal: Correlation of motion noise in the calculated TMI is hardly detectable after application of one of the calibration methods to the magnetometer signals. The correlation coefficients for the particular data are of the magnitude of one per thousand for the roll angle and in the percentage range for pitch and heading. This addresses correlations between pitch, heading and topography and is not subject to magnetometer calibration.

For larger data sets with a larger number of survey flights the almost negligible differences in the scaling and misalignment behaviour of the magnetometer system should be kept in mind. After calibration of each separate flight (line) individually, the scale factors and misalignment angles could be averaged, and subsequently the offsets estimated by recalibration with fixed values for $s_i$ and $\alpha_{ij}$. A single set of $s_i$ and $\alpha_{ij}$ for a specific survey exists as well as the offsets for each flight line after proper calibration.

The ellipsoid method after (Merayo *et al.* 2000) instead is more robust to minimization for offset determination, but a common reference coordinate frame for the measured data and the Earth's magnetic field components is necessary. Secondly, the calibration routine is faster than Olsen's method *et al.* (2001) but only a raw calibration model for the offset and scale factor determination is used. Hence, the influence of motion noise on the resulting TMI remains stronger than for Olsen's routine. Application of the same minimizer (L-BFGS) for solving this task would result in a longer computing time. Thirdly, it is necessary to estimate the misalignment of the magnetometer triplet relative to the IMU because this causes further distortions. This step has to be performed via a minimization routine during the calibration procedure. However, it results in an increased calculating time spent for the optimization. Furthermore, depending on the minimization algorithm, convergence to realistic values is not always secured.

With appropriate offset scaling, especially the Olsen method has the potential to be used for calibration of a wide range of SQUID vector magnetometer survey data.

## 7 CONCLUSION AND OUTLOOK

Initially thought to be more robust for typical SQUID vector magnetometer setups, the calibration after Merayo and Bonnet turns out to have several disadvantages because the offsets and scale values have to be pre-calibrated. Olsen's *et al.* (2001) however, allows calibrating the vector magnetometer itself and determining its alignment to the IMU coordinate system. The orientation of the whole tri-axial setup relative to the IMU coordinate system is determined afterwards. An appropriate rescaling of the offset values during the calibration process enhances the stability of the algorithm and the quality of the resulting TMI values for the surveyed. The evaluation of the methods, as presented in this paper, is based on comparisons with a reference field TMI derived from IGRF or HDGM spherical harmonics coefficients. However, better a priori TMI data used for calibration may improve the stability.

In regard to the FTMG system setup used for the example data presented here, we intend to publish a future approach for the generation of a correct reference field, which utilizes magnetic field components that can be calculated from the vertical components of the gradient tensor ($B_{xz}$, $B_{yz}$ and $B_{zz}$) under Hilbert and Hilbert-like transforms.

## ACKNOWLEDGEMENTS

The authors thank the team at AngloAmerican and DeBeers for their friendly permission to use the data for this manuscript.

This work is a part of INFLUINS, a high performance research project granted by the German Federal Ministry of Education and Research (BMBF) under grant no. 03IS2091-A,C,F.

## REFERENCES

Alonso, R. & Shuster, M.D., 2002. Complete linear attitude-independent magnetometer calibration, *J. Astron. Sci.,* **50,** 477–490.

Barraud, A. & Lesecq, S., 2008. *Magnetometer Calibration*, MathWorks® Available at: http://www.mathworks.com/matlabcentral/fileexchange/23398-magnetometers-calibration (last accessed 16 March 2012).

Barrow, B. & Nelson, H.H., 1998. Collection and analysis of multi-sensor ordnance signatures with MTADS, *J. Environ. Eng. Geophys.*, **3,** 71–79.

Bick, M. *et al.*, 1999, A HTS rf SQUID vector magnetometer for geophysical exploration, *IEEE Trans. Appl. Superconduct.*, **9,** 3780–3785.

Bonnet, S., Bassompierre, C., Godin, C., Lesecq, S. & Barraud, A., 2009 Calibration methods for inertial and magnetic sensors, *Sens. Actuat. A*, **156,** 302–311.

Broyden, C.G., 1970. The convergence of a class of double-rank minimization algorithms, *J. Inst. Math. Applicat.*, **6,** 76–90.

Burghoff, M. *et al.*, 2004. Discrimination of multiple sources using a SQUID vector magnetometer, *Neurol. Clin. Neurophysiol.*, **67,** 1–2.

Clark, A.J., 1996. *Seeing Beneath the Soil: Prospecting Methods in Archaeology*, B.T. Batsford Ltd.

Clarke, J. & Braginski, A.I., 2004. *The SQUID Handbook*, Vol. 1: *Fundamentals and Technology of SQUIDs and SQUID Systems,* Wiley VCH.

Crous, S.P., 1997. The geology, geochemistry and geophysics of the Southeastern Flank of the Dennilton Dome, Northern Province, South Africa: implications for exploration, in *Proceedings of Exploration 1997: Fourth Decennial International Conference on Mineral Exploration*, Toronto, Canada, pp. 851–856, ed. Gubins, A.G., Prospectors and Developers Association of Canada (PDAC).

Finlay, C.C. *et al.*, 2010. International geomagnetic reference field: the eleventh generation, *Geophys. J. Int.*, **183,** 1216–1230.

Goldstein, H., 1980. *Classical Mechanics*, 2nd edn, Addison–Wesley.

Gray, A., 1997. *Modern Differential Geometry of Curves and Surfaces with Mathematica*, 2nd edn, CRC Press.

Jacobs, J.A., 1987. *Geomagnetism*, Vol. 1, Academic Press Ltd.

Linzen, S., Schultze, V., Chwala, A., Schüler, T., Schulz, M., Stolz, R. & Meyer, H.-G., 2009. Quantum detection meets archaeology—magnetic prospection with SQUIDs, highly sensitive and fast, in *New Technologies for Archaeology*, pp. 71–85, eds Reindel, M. & Wagner, G.A., Springer.

Macnae, J.C., 1979. Kimberlites and exploration geophysics, *Geophysics*, **44,** 1395–1416.

Marklund, G.T., Blomberg, L.G. & Persson, S., 2001. Astrid-2, an advanced microsatellite for auroral research, *Ann. Geophys.*, **19,** 589–592.

Maus, S. & Manoj, C., 2010. Geomagnetic field models for exploration and directional drilling, *SEG Expanded Abstr.*, **30,** 2344–2347.

Maus, S. & Manoj, C., 2012. High definition geomagnetic models: a new perspective for improved wellbore positioning, in *Proceedings of the IADC/SPE Drilling Conference and Exhibition,* San Diego, CA, IADC/SPE-151436-PP 1–15.

Merayo, J.M.G., Brauer, P., Primdahl, F., Petersen, J.R. & Nielsen, O.V., 2000. Scalar calibration of vector magnetometers, *Measure. Sci. Technol.*, **11,** 120–123.

Munschy, M., Boulanger, D., Ulrich, P. & Bouiflane, M., 2007. Magnetic mapping for the detection and characterization of UXO: use of multisensor fluxgate 3-axis magnetometers and methods of interpretation, *J. appl. Geophys.*, **61,** 168–173.

Nelson, H.H. & McDonald, J.R., 2001. Multisensor towed array detection system for UXO detection, *IEEE Trans. Geosci. Remote Sens.*, **39,** 1139–1145.

NGDC (National Geophysical Data Center), 2012a. Initial Geomagnetic Reference Field. Available at: http://www.ngdc.noaa.gov/IAGA/vmod/igrf.html (last accessed 12 May 2012).

NGDC (National Geophysical Data Center), 2012b. Spherical harmonic coeffcients for the High Definition Geomagnetic Model. Available at: http://geomag.org/models/NGDC-720/NGDC-720_V3p1.cof.gz (last accessed 12 May 2012).

Olsen, N., Toffner-Clausen, L., Risbo, T., Brauer, P., Merayo, J., Primdahl, F. & Sabaka, T., 2001. In-flight calibration methods used for the Ørsted mission, in *Ground and In-Flight Space Magnetometer Calibration Techniques, ESA SP-490*, pp. 1–13, eds Balogh, A. & Primdahl, F., ESA Publishing Division, ESTEC, Katwijk, The Netherlands.

Sabaka, T.J., Olsen, N. & Purucker, M.E., 2004. Extending comprehensive models of the Earth's magnetic field with Ørsted and CHAMP data, *Geophys. J. Int.*, **159,** 521–547.

Schmidt, M., 2012. minFunc—unconstrained differentiable multivariate optimization in MATLAB, Available at: http://www.di.ens.fr/~mschmidt/Software/minFunc.html (last accessed 20 September 2011).

Schmidt, P.W. & Clark, D.A., 2000. Advantages of measuring the magnetic gradient tensor, *Preview*, **85,** 26–30.

Schnabel, A., Burghoff, M., Hartwig, S., Petsche, F., Steinhoff, U., Drung, D. & Koch, H., 2004. A sensor configuration for a 304 SQUID vector magnetometer, *Neurol. Clin. Neurophysiol.*, **70,** 1–4.

Shin, E.-H., 2005, Estimation techniques for low-cost inertial navigation, *PhD dissertation*, University of Calgary, Calgary.

Shin, E.-H. & El-Sheimy, N., 2007. Unscented kalman filter and attitude errors of low-cost inertial navigation systems, *Navigation*, **54,** 1–9.

Stolz, R., 2006. Supraleitende Quanteninterferenzdetektor-Gradiometer-Systeme für den geophysikalischen Einsatz, *PhD thesis*, Isle Verlag, Ilmenau.

Stolz, R., Fritzsch, L. & Meyer, H-G., 1999. LTS SQUID sensor with a new configuration, *Supercond. Sci. Technol.*, **12**(11), 806–808.

Stolz, R., Zakosarenko, V., Schulz, M., Chwala, A., Fritzsch, L., Meyer, H.G. & Köstlin, E.O., 2006. Magnetic full-tensor SQUID gradiometer system for geophysical applications, *Leading Edge*, **25,** 178–180.

Vrba, J., 1996. SQUID gradiometers in real environments, in *NATO ASI Series E: Applied Sciences, SQUIDs: Fundamentals, Fabrication and Applications*, pp. 117–178, ed. Weinstock, H., Kluwer Academic Publishers, Dordrecht, The Netherlands.